

High Fidelity Theta Phase Rolling of CA1 Neurons

Hadas E. Sloin, Amir Levi, Shirly Someck, Lidor Spivak, and Eran Stark

Sagol School of Neuroscience and Department of Physiology and Pharmacology, Sackler Faculty of Medicine, Tel Aviv University, Tel Aviv 6997801, Israel

Single hippocampal cells encode the spatial position of an animal by increasing their firing rates within “place fields,” and by shifting the phase of their spikes to earlier phases of the ongoing theta oscillations (theta phase precession). Whether other forms of spatial phase changes exist in the hippocampus is unknown. Here, we used high-density electrophysiological recordings in mice of either sex running back and forth on a 150-cm linear track. We found that the instantaneous phase of spikes shifts to progressively later theta phases as the animal traverses the place field. We term this shift theta “phase rolling.” Phase rolling is opposite in direction to precession, faster than precession, and occurs between distinct theta cycles. Place fields that exhibit phase rolling are larger than nonrolling fields, and in-field spikes occur in distinct theta phases in rolling compared with nonrolling fields. As a phase change associated with position, theta phase rolling may be used to encode space.

Key words: extracellular recordings; hippocampus; phase code; phase precession; pyramidal neurons; spatial navigation

Significance Statement

Theta phase precession is a well-known coding scheme in which neurons represent the position of the animal by the timing of their spikes with respect to the phase of ongoing theta oscillations. Here, we show that hippocampal neurons also undergo “theta phase rolling,” a phase change faster and opposite in direction to precession. As the animal advances in space, spikes occur at progressively later phases of consecutive theta cycles. Future studies may reveal whether phase rolling constitutes a novel coding mechanism of space.

Introduction

How neurons encode information is a major question in systems neuroscience (Bialek et al., 1991; deCharms and Zador, 2000; Stanley, 2013). Single neurons carry information by their firing rates (Adrian and Zotterman, 1926; Barlow, 1972; Azarfar et al., 2018) or by the precise timing of spikes in relation to a reference. The reference can be another spike of the same neuron (Reich et al., 2000; Imaizumi et al., 2010) or an external event (Optican and Richmond, 1987; Chase and Young, 2007). Neuronal assemblies also carry information by spatiotemporal patterns of activation (Gray et al., 1989; Graf et al., 2011; Kohn et al., 2016). Unfortunately, only a small fraction of all neurons in each network can be monitored at a given time. However, the activity of

a population of neurons can be estimated by local field potentials (LFPs), a measure of the summed electric fields created by the synaptic activity of many neurons (Buzsáki et al., 2012; Herreras, 2016). LFP signals often consist of periodic oscillations at discrete frequency bands (Buzsáki and Draguhn, 2004; Singer, 2018) which can be used to define an internal reference to spikes. In such “phase coding,” information is carried by the timing of the spikes of a single neuron in relation to ongoing LFP oscillations (Montemurro et al., 2008; Turesson et al., 2012; Siadatnejad et al., 2013). Thus, a phase code is a type of a temporal assembly code, in which the activity of one neuron is referred to the synchronized activity of many hidden neurons, represented by the LFP oscillations.

Rate and phase coding by spiking neurons have been studied extensively in the context of spatial representation in the hippocampus (Hartley et al., 2014). Hippocampal neurons called “place cells” encode space by firing at elevated rates when the animal is in a specific region, the place field (O’Keefe and Dostrovsky, 1971; Moser et al., 2008). Many cells also encode information by the timing of spikes in relation to the instantaneous phase of hippocampal theta oscillations (Vanderwolf, 1969; Lever et al., 2014). As the animal traverses the place field, spikes occur at progressively earlier theta phases (O’Keefe and Recce, 1993; Skaggs et al., 1996). This phase code, termed “theta phase precession,” carries spatial information in addition to that carried by the rate code, improving the accuracy of the inferred

Received Oct. 28, 2021; revised Feb. 15, 2022; accepted Feb. 17, 2022.

Author contributions: H.E.S. and E.S. designed research; H.E.S. and E.S. performed research; H.E.S., A.L., S.S., and E.S. contributed unpublished reagents/analytic tools; H.E.S., A.L., S.S., L.S., and E.S. analyzed data; H.E.S. and E.S. wrote the first draft of the paper; H.E.S., A.L., S.S., L.S., and E.S. edited the paper; H.E.S. and E.S. wrote the paper.

This work was supported by the Israel Science Foundation Grant #638/16, the European Research Council Grant #679253, and by the Canadian Institutes of Health Research (CIHR), the International Development Research Centre (IDRC), the Israel Science Foundation (ISF) and the Azrieli Foundation Grant #2558/18. We thank Ortal Amber-Vitos for establishing and managing the animal colony and Leore Heim for help collecting preliminary data. We also thank Kamran Diba, Shaked Palgi, and Meishar Shahoha for constructive comments.

The authors declare no competing financial interests.

Correspondence should be addressed to Eran Stark at eranstark@tauex.tau.ac.il.

<https://doi.org/10.1523/JNEUROSCI.2151-21.2022>

Copyright © 2022 the authors

Table 1. List of experimental animals

Animal ID	Sex	Age ^a (week)	Weight (g)	Probe	Sessions	Trials ^b	All PYR	Active PYR ^c	All INT	Active INT ^c
mC41	M	10	33.7	Stark64	33	194 [158 246]	1972	557	400	212
mA234	M	16	30	Buzsaki32	24	170 [134 206]	1440	446	206	135
mP23	M	15	31.2	Buzsaki32	14	116 [98 140]	295	81	48	26
mDS1	M	14	25.7	Dual-sided64	5	136 [120 140]	222	54	27	13
mDS2	F	30	24.2	Dual-sided64	21	160 [130 182]	1732	790	228	155
Total					97		5661	1928	909	541

^aAt time of implantation.^bNumber of one-direction trials, median [IQR].^cWell-isolated PYR/INT, active and stable on the linear track.

position of the animal (Jensen and Lisman, 2000; Reifenstein et al., 2012). Originally described in CA1 pyramidal cells (PYR), precession has also been described in CA1 interneurons (INT; Maurer et al., 2006; Ego-Stengel and Wilson, 2007), and is found in other hippocampal regions (O’Keefe and Recce, 1993; Tsodyks et al., 1996) as well as in nonhippocampal regions (Van Der Meer and Redish, 2011; Tingley et al., 2018).

To date, theta phase precession is the only thoroughly studied spatial theta phase code. Yet a priori, multiple other phase codes are possible. Even precession itself is not a purely linear phase shift and is often asymmetric. In the second half of the place field, the slope of precession decreases (Mehta et al., 2002) and the variability of the phase increases (Ceï et al., 2014; Souza and Tort, 2017). In some cases, the slope of precession reverses to generate “precession” in the second part of a place field (Yamaguchi et al., 2002; Wang et al., 2020). Interneurons occasionally exhibit a positive phase shift, in which theta phase advances forward (Ego-Stengel and Wilson, 2007). Positive phase shifts were also reported in small fractions of cells recorded from the lateral septum and the hippocampus (Monaco et al., 2019).

To determine whether there are additional phase-position patterns in CA1, we used high-density extracellular recordings in freely-moving mice. We found that CA1 neurons undergo a previously undescribed phase shift that we term “theta phase rolling.” Akin to precession, phase rolling occurs with respect to the ongoing theta oscillations but is faster and opposite in direction to precession.

Materials and Methods

Experimental design

Experimental animals

Three freely moving C57BL/NJ mice and two hybrid C57BL/NJ x FVB/NJ mice (mC41 and mA234) were used in this study (Table 1). Four of the mice were males and one was female, aged 10–30 weeks at the time of implantation. Animals were healthy, were not involved in previous procedures, and weighed 24.2–33.7 g at the time of implantation. Mice were single housed to prevent damage to the implanted apparatus. All animal handling procedures were in accordance with Directive 2010/63/EU of the European Parliament, complied with Israeli Animal Welfare Law (1994), and approved by Tel Aviv University Institutional Animal Care and Use Committee (IACUC; #01-16-051).

Probes and surgery

Every animal was implanted with a multi-shank silicon probe attached to a movable microdrive and coupled with optical fibers following previously described procedures (Stark et al., 2012; Noked et al., 2021). The probes used were Stark64 (Diagnostic Biochips), Buzsaki32 (NeuroNexus), and Dual-sided64 (Diagnostic Biochips). The Stark64 probe consists of six shanks, spaced horizontally 200 μm apart, with each shank consisting of 10–11 recording sites,

spaced vertically 15 μm apart. The Buzsaki32 probe consists of four shanks, spaced horizontally 200 μm apart, with each shank consisting of eight recording sites, spaced vertically 20 μm apart. The Dual-sided64 probe consists of two dual-sided shanks, spaced horizontally 250 μm apart, with each shank consisting of 16 channels on each side (front and back), spaced vertically 20 μm apart.

Probes were implanted in the neocortex above the right hippocampus (PA/LM, 1.6/1.1 mm; 45° angle to the midline) under isoflurane (1%) anesthesia. After recovery from anesthesia, animals were placed on a water-restriction schedule that guaranteed at least 40 ml/kg of water (corresponding to 1 ml per 25-g mouse) on every recording day. Recordings were conducted 5 d/week, and animals received free water on the sixth day. After every one to five recording sessions, the probe was translated vertically downwards by up to 70 μm. Analyses included only recordings from the CA1 pyramidal cell layer, recognized by the appearance of multiple high-amplitude units and iso-potential spontaneous ripple events.

Behavior and recording sessions

Neuronal activity was recorded in 4.5 [1.9 10.1] h sessions (median [interquartile range, IQR]). At the beginning of every session, neural activity was recorded while the animal was in the home cage. The animal was then placed on a 150-cm linear track that extended between two 10 × 10-cm square platforms. Each platform included a water delivery port. Mice were under water restriction and were trained to repeatedly traverse the track for a water reward of 3–10 μl. Mice ran 167 [131.5 200.24] one-direction trials over about 1 h (Table 1). Trials in which the mean running speed was below 10 cm/s were excluded from analyses. Animals were equipped with a 3-axis accelerometer (ADXL-335, Analog Devices) for monitoring head movements. Head position and orientation were tracked in real time using two head-mounted LEDs, a machine vision camera (ace 1300-1200uc, Basler), and a dedicated system (“Spotter,” Gaspar et al., 2019).

Spike detection and sorting

Neural activity was filtered, amplified, multiplexed, and digitized on the headstage (0.1–7500 Hz, x192; 16 bits, 20 kHz; RHD2132 or RHD2164, Intan Technologies), and then recorded by an RHD2000 evaluation board (Intan Technologies). Offline, spikes were detected and sorted into single units automatically using KlustaKwik3 (Kadir et al., 2014; Rossant et al., 2016) for shanks with up to 11 sites/shank, or KiloSort2 (Pachitariu et al., 2016) for 16 channel shanks. Automatic spike sorting was followed by manual adjustment of the clusters. Only well-isolated units were used for further analyses [amplitude >40 μV; L-ratio <0.05 (Schmitzer-Torbert et al., 2005); inter-spike interval index <0.2 (Fee et al., 1996)]. Units were classified into putative PYR or PV-like INT using a Gaussian mixture model (Stark et al., 2013). A total of 5661 PYRs and 909 INTs were recorded from CA1 of the five freely moving mice.

Linear track firing rates

To create trial-averaged firing rate maps (Fig. 1B), we defined a “trial” as a single run across the linear track, either left-to-right or right-to-left. Time segments that occurred while the speed of the animal was below 10 cm/s were omitted. The firing rate in each trial was binned into 2.5-cm spatial bins, and count and temporal occupancy maps were calculated and smoothed with a Gaussian kernel that had an SD of 5 cm. A

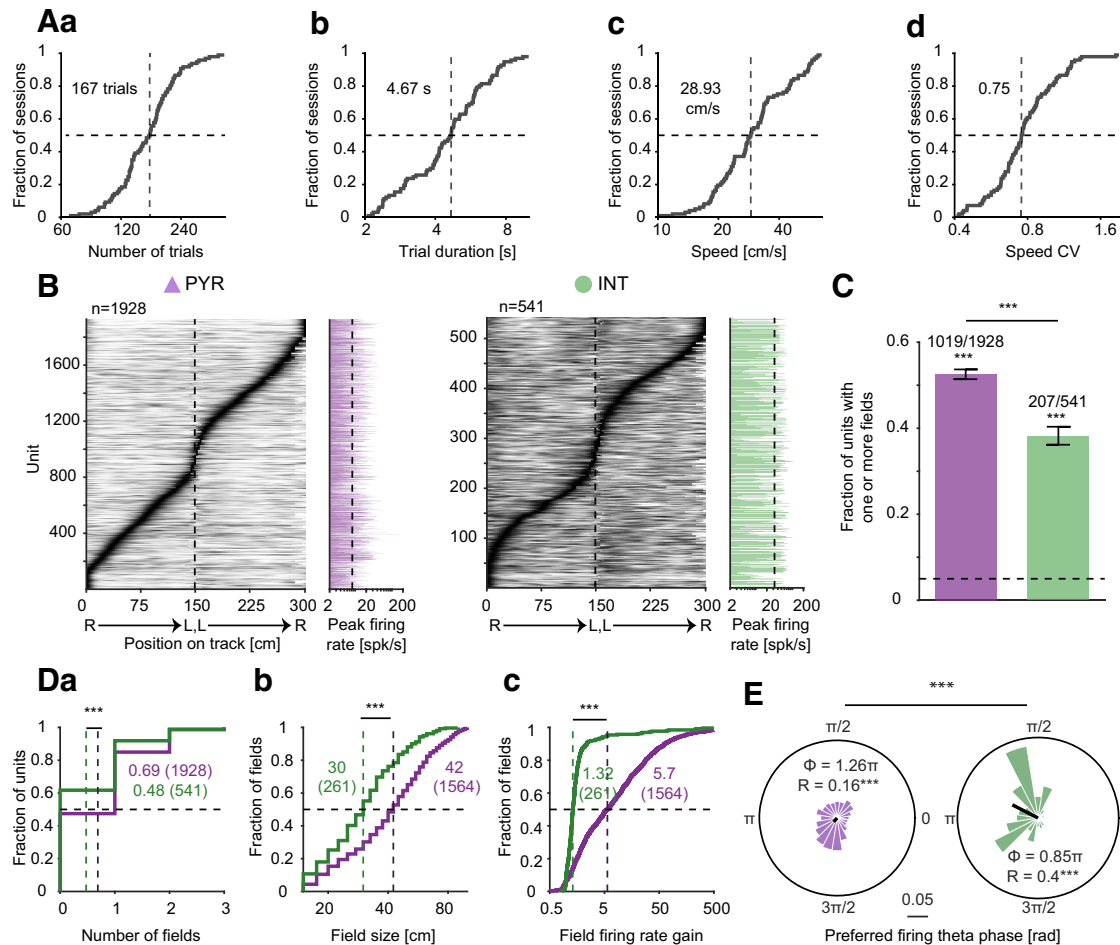


Figure 1. CA1 pyramidal cells and interneurons exhibit place fields, but pyramidal cells exhibit higher in-field firing rate gain. **A**, Movement kinematics during $n = 97$ recording sessions, as five mice ran back and forth on a 150-cm-long linear track. **a**, Number of left-to-right and right-to-left trials. Here and in subpanels **b–d**, dashed lines show group medians. **b**, Mean trial duration. **c**, Mean running speed over trials. **d**, Speed coefficient of variation (CV), defined as the speed SD divided by the mean speed over trials. **B**, Firing rate maps of active and stable putative CA1 pyramidal cells (PYR) and interneurons (INT). Each row represents a unit; firing rates on right (R) to left (L) runs were concatenated with L to R runs and scaled to the 0–1 (white-black) range for presentation purposes. Right, Peak on-track firing rate. **C**, Fraction of PYR and INT with one or more place fields out of all units active and stable on the track. $***p < 0.001$, binomial test, comparing to chance level (0.05; horizontal dashed lines). Error bars show SEM. The fraction of units with one or more fields is larger among PYR ($***p < 0.001$, G test). **D**, Place field properties of CA1 PYR and INT. **a**, Number of place fields of each unit ($***p < 0.001$, U test). Dashed lines show group means. The mean of each group is indicated, followed in parentheses by the number of fields per group. **b**, Place field size of all PYR and INT fields. Here and in subpanel **c**, vertical dashed lines show group medians; the median of each group is indicated, followed in parentheses by the number of fields per group. **c**, In-field firing rate gain, defined as the ratio between mean within-field firing rate and the mean firing rate outside the place field. **E**, Preferred theta phase of firing does not distribute uniformly in both PYR and INT ($***p < 0.001$, Rayleigh test). The preferred theta phase is different among PYR and INT fields ($***p < 0.001$, Wheeler test). Phases are binned into 20 equally sized bins. Scale bar corresponds to a probability of 0.05. The mean phase (ϕ) and resultant length (R) are denoted by the line at the center of the histogram and are indicated in text.

firing rate map was constructed for each trial by dividing the count map by the temporal occupancy map. Finally, a trial-averaged firing rate map was constructed for each run direction separately by calculating the mean firing rate in every spatial bin, weighted by the value in the corresponding bin of the occupancy map.

Activity and stability criteria

Many of the recorded units did not fire while the animal was on the linear track. Other units exhibited unstable firing during track sessions. All the analyses in the current study were performed only on active and stable units. Units that fired at least 5 spikes in at least one 2.5-cm spatial bin, pooled over all trials, were considered active. A total of 3722/5661 PYR (61%) and 753/909 (79%) INT were active. To quantify stability, for each unit we calculated the rank correlation coefficient (cc) between the firing rate maps of all same-direction trial pairs. For every trial pair, statistical significance was estimated using a permutation test. The overall p -value was estimated by the geometric mean over all pairs in both running directions. Units with consistent cc were considered stable. A total of 1928/3722 (51%) active PYRs and 541/753 (72%) active INTs were stable.

Identification of place fields

Typically, place fields are defined as continuous regions in which the firing rate of a PYR is above 10–20% of the peak on-track firing rate (Schmidt et al., 2009; Mizuseki et al., 2011; Diamantaki et al., 2018). However, such definitions assume discrete firing fields and do not attach a probability value to each field. Furthermore, INT change their firing rate according to position, exhibiting “on” and “off” regions on the track (Maurer et al., 2006; Ego-Stengel and Wilson, 2007; Wilent and Nitz, 2007; Hangya et al., 2010). Yet peak firing rate methods do not allow the identification of INT spatial firing regions. To detect place fields in a rigorous statistical manner in both PYR and INT, we developed a method based on Poisson distributions for field detection. In the Poisson method, place fields are defined as regions in which the firing rate deviates from chance at a given level of probability. For that, an estimate of the on-track spontaneous mean firing rate λ of each unit is required. However, the mean firing rate cannot be estimated based on off-track spiking, since many units rarely fire off-track. On the other hand, the mean on-track firing rate is strongly biased upwards by spatial spiking. To balance these two opposing biases, we used an iterative approach for estimating λ :

1. Trial-averaged firing maps were calculated separately for right-to-left and left-to-right trials.
2. Initially, λ was defined as the mean firing rate over all right-to-left and left-to-right bins, weighted by the total occupancy time in each bin.
3. The mean firing rate in each bin was compared to λ . Outlier bins were defined as bins in which the Poisson probability to obtain the observed firing rates or higher (if the firing rate was larger than λ) or lower (if the firing rate was smaller than λ), was higher than expected by chance. The alpha level was Bonferroni corrected for the number of effectively independent bins, determined by the full-width at half-height of the autocorrelation of the firing-rate map.
4. λ was recalculated after excluding the outlier bins.
5. Steps 3–4 were repeated for five iterations. Initial testing showed that five iterations are sufficient for convergence.

After establishing λ for a given unit, we determined whether the unit exhibited one or more place fields. For that, we again estimated the Poisson probability to obtain the observed (or higher) mean firing rates in each spatial bin of the rate map, given λ . Place fields were identified as regions of 15–100 cm with above-chance firing rates. Finally, place fields that contained a total of <30 spikes were omitted from further analyses, since preliminary testing showed that circular-linear analyses of phase changes (see below) are unreliable when the number of spikes is smaller. Overall, a total of 1564 PYRs and 261 INTs place fields were identified in 1928 PYR and 541 INT units (Table 1).

As a control for results obtained using the Poisson field detection method, we also detected “classical” fields using a procedure employed in multiple previous studies (Schmidt et al., 2009; Mizuseki et al., 2011; Diamantaki et al., 2018; Sharif et al., 2021). Classical fields were defined as (1) continuous regions spanning at least 15 cm; (2) in which the firing rate is above 10% of the peak rate in the field; and (3) exhibit a peak firing rate of at least two spikes per second. The classical method yielded 1636 PYR fields ($p = 0.93$, G test). Out of 1564 PYR fields identified by the Poisson method, 1009 (65%) overlapped fields identified by the classical method by at least 50% of the Poisson field. As expected, the two methods yielded considerably different INT fields: the classical method identified only 22 fields in 541 INTs, whereas 261 fields were identified by the Poisson method. To determine whether the detection of phase rolling (see below) depends on the field identification method, we repeated analyses for spikes within classical fields. 555/1636 (34%) of the classical fields exhibited phase rolling, compared with 540/1564 (34%) of the Poisson fields ($p = 0.8$, G test). Of the 540 Poisson fields that exhibited rolling, 432 (80%) also exhibited fields according to the classical method. Of these, 298/432 (69%) fields exhibited rolling also according to the classical method (chance level, 11.7%; $p < 1.11 \times 10^{-16}$, exact binomial test). Furthermore, 258/1636 (16%) of the classical PYR fields exhibited between-cycle rolling, compared with 241/1564 (15%) of the Poisson fields ($p = 0.81$, G test). Of the 241 Poisson fields that exhibited between-cycle rolling, 184 (76%) also exhibited fields according to the classical method. Of these, 101/184 (55%) fields exhibited rolling by both methods (chance level, 2.4%; $p < 1.11 \times 10^{-16}$, exact binomial test).

Instantaneous theta phase

To estimate the instantaneous phase of theta oscillations, one CA1 pyramidal cell layer channel was chosen for each session. The theta reference was the channel that exhibited the best signal-to-noise ratio (SNR), defined as the theta (5–11 Hz) to δ (2–4 Hz) power ratio (“SNR” method). The theta phase at each time point was calculated using the waveform method (Belluscio et al., 2012; Maurer et al., 2014). The LFP from the CA1 PYR channel was filtered with a zero-phase two-pole Butterworth bandpass (1–60 Hz) filter. The local maxima and minima of the filtered signal were determined, and extrema closer than 71 ms (14 Hz) were pruned. Each peak was assigned a phase of 0 rad, and each trough was assigned a phase of π rad. Phases at all other time points were interpolated linearly between peaks and troughs. To minimize discontinuities, the interpolated phases were smoothed using a Gaussian low-pass filter with a corner frequency of 13.6 [13.4–14.7] Hz (corresponding to half the mean session-specific theta cycle duration). Every spike

was assigned the theta phase that occurred at the time of the spike, referred to as “spike phase.”

As a control for the theta channel selection method, we used a theta reference channel from the center of the CA1 pyramidal cell layer (“CA1pyr” method). The center of the layer was identified for each shank by the channel with iso-potential spontaneous ripple events (Ylinen et al., 1995). For each session, the shank with the maximal power between 130 and 190 Hz was selected. For on-track instantaneous phases, the mean \pm SD difference between the theta reference based on the SNR and the CA1pyr methods was $0.047\pi \pm 0.33\pi$ rad. Out of 1564 PYR fields, 540 (34%) exhibited phase rolling (see below) using the SNR method, compared with 526 (34%) using the CA1pyr method ($p = 0.71$, G test); 378/540 (70%) fields exhibited rolling by both methods (chance level, 11.6%; $p < 1.11 \times 10^{-16}$, exact binomial test). Furthermore, 241 (15%) PYR fields exhibited between-cycle rolling using the SNR method, compared with 230 PYR fields using the CA1pyr method (15%; $p = 0.9$, G test); 109/241 (45%) fields exhibited between-cycle rolling by both methods (chance level, 2.3%; $p < 1.11 \times 10^{-16}$, exact binomial test). There was no consistent difference in the fraction of PYR fields undergoing precession between the two methods (power: 799/1564, layer: 821/1564, $p = 0.66$, G test). In multiple previous reports (Hafting et al., 2008; Royer et al., 2012; Sharif et al., 2021), theta phase was estimated by applying a narrow bandpass filter (5–11 Hz) followed by Hilbert transform. To determine whether filtering specifics affect the detection of phase rolling, we repeated the rolling analysis following narrow-band filtering. Out of 1564 PYR fields, 540 (34%) fields exhibited rolling following 1- to 60-Hz filtering, compared with 595 (38%) following 5- to 11-Hz filtering ($p = 0.16$, G test). 395/540 (73%) fields exhibited rolling following filtering at both bands (chance level, 13.1%; $p < 1.11 \times 10^{-16}$, exact binomial test); 241 (15%) PYR fields exhibited between-cycle rolling following 1- to 60-Hz filtering, compared with 229 (15%) following 5- to 11-Hz filtering ($p = 0.93$, G test). A total of 96/241 (40%) fields exhibited between-cycle rolling following filtering at both bands (chance level, 2.3%; $p < 1.11 \times 10^{-16}$, exact binomial test). Thus, the precise theta reference channel and filtering range do not consistently affect rolling prevalence.

Theta phase lock, precession, and rolling

To quantify on-track spike theta phase locking within each place field, we calculated the mean phase of all the spikes that occurred in the field. Phase locking fit was quantified using the length of the circular resultant vector ($R = |\vec{R}|$) and tested using Rayleigh’s likelihood-ratio test of uniformity.

Theta phase precession and phase rolling were quantified for each place field by a circular-linear analysis (Schmidt et al., 2009; Kempter et al., 2012). To quantify theta phase changes, we fitted a line to the instantaneous theta phase of each spike, $\theta(x)$, and the spatial position of the animal at spike time, x : $\hat{\theta}(x) = \theta_0 + 2\pi ax$, where a is the slope and θ_0 is the phase offset. For each slope a in the tested range (see below), we first calculated the angular residuals of the circular-linear model: $\varepsilon(x) = \theta(x) - \hat{\theta}(x) = \theta(x) - (\theta_0 + 2\pi ax)$. We then calculated the resultant length (R) of the residuals, indicating model fit. The fitted slope a was the slope that yielded the largest R , corresponding to the slope for which the variance of the residuals was smallest. The value of the maximal resultant length was used to indicate the fit of the circular-linear model. Statistical significance of the optimized model was estimated by randomly permuting the $\{\theta(x), x\}$ pairs.

Preliminary observations suggested that the same unit may simultaneously exhibit theta phase locking, precession, and phase rolling. However, the circular-linear analysis yields a single optimum, potentially causing one phenomenon to shadow another. Circular-linear analysis is especially problematic in the presence of phase locking, as often observed for INT (Csicsvari et al., 1999; Frank et al., 2001; Klausberger et al., 2003; Somogyi and Klausberger, 2005). If the range of slopes used for the circular-linear analysis includes zero (a horizontal line), the zero-slope may yield the best fit for a phase-locked unit, even if that unit co-exhibits phase changes. To enable detecting multiple phase phenomena

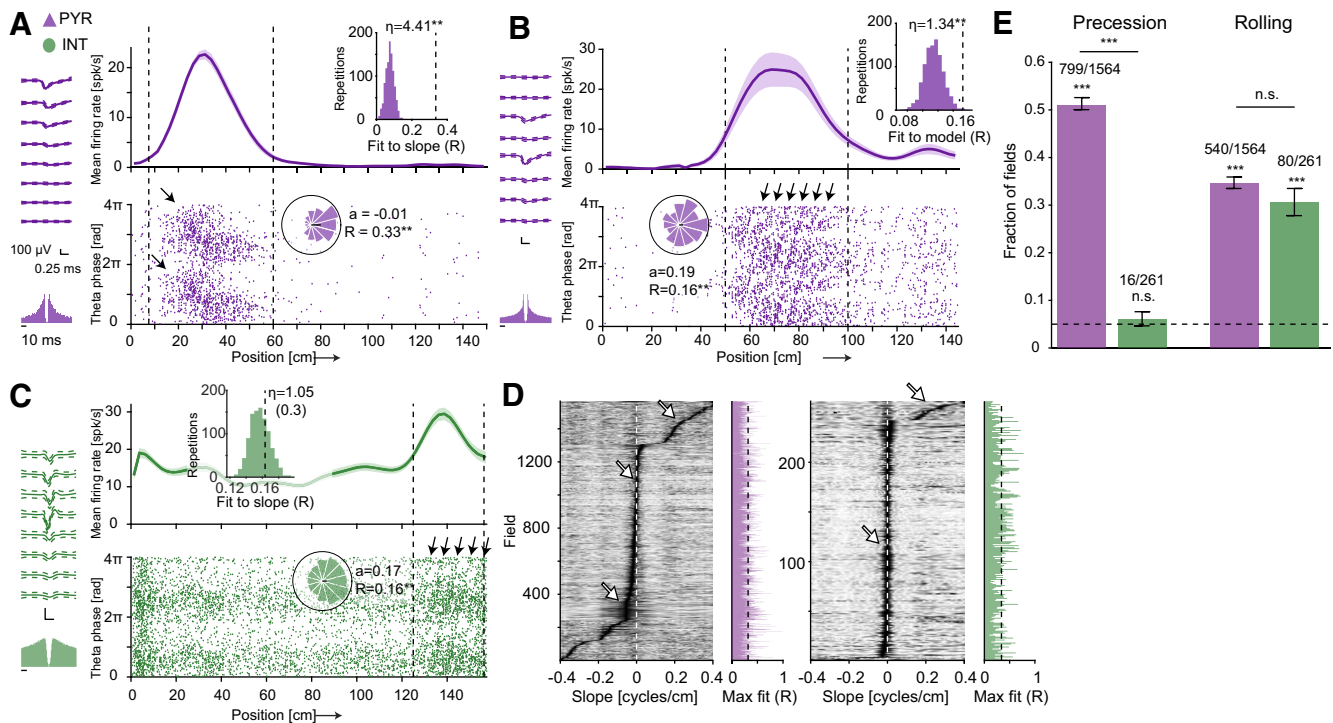


Figure 2. CA1 pyramidal cells and interneurons exhibit theta phase rolling. **A**, An example PYR, exhibiting theta phase precession: a negative slope of phase changes with respect to advanced position on the track. Top, Firing rate as a function of position (mean \pm SEM across 46 same-direction trials). Top inset, Distribution of precession fit values for phase-randomized spikes (see Fig. 3). Bottom, Instantaneous theta phase of every spike, plotted as a function of animal position at spike time. Phase $0/\pi$ corresponds to theta peak/trough. Running direction is presented from left to right, and vertical dashed lines indicate place field limits. Phase precession slope a was determined by fitting a circular-linear model to the spike phases at each position in the field (** $p < 0.01$, permutation test). Arrows indicate phase precession. Bottom inset, Circular distribution of the residuals of the circular-linear model; the resultant length R of the residuals indicates the goodness of fit. Left, Wide-band (0.1–7500 Hz) spike waveforms (mean \pm SD) recorded on eight consecutive sites (20- μ m intersite vertical spacing) and autocorrelation histogram. **B**, An example PYR, exhibiting theta phase rolling: a positive slope of phase changes with respect to advanced position on the track. Activity was recorded across 37 same-direction trials. All conventions are the same as in panel **A**. **C**, An example INT, exhibiting theta phase rolling. Activity was recorded across 57 same-direction trials. All conventions are the same as in panel **A**. **D**, For every place field (1564 PYR and 261 INT fields), the slope of a circular-linear model was varied systematically, and the resultant length (R) of the residuals calculated. Each row shows the R values corresponding to multiple models (slopes) fitted to one field. R values are scaled to the 0–1 range for presentation purposes. Arrows indicate qualitatively different subsets of fields. In each subset, a different spike phase phenomenon is most evident. Bottom, Phase precession. Middle, Phase locking. Top, Phase rolling. **E**, Theta phase rolling occurs in both PYR and INT. Fraction of PYR and INT fields with theta phase precession ($p < 0.05$, permutation test; left two bars), or theta phase rolling ($p < 0.05$, permutation test; right bars) out of all place fields. Horizontal dashed lines show chance level (0.05), and error bars show SEM. The fraction of fields with phase precession/rolling is above expected by chance in all cases (** $p < 0.001$, exact binomial test), except for INT precession ($p = 0.24$). Precession is more prevalent among PYR than among INT (** $p < 0.001$, G test), while phase rolling prevalence does not differ between cell types (not significant (n.s.): $p = 0.38$).

in a single field, we tested each place field for two circular-linear models. Negative slopes (corresponding to potential phase precession) were optimized in the range between $\tan(-0.1)$ and $\tan(-0.005)$ cycles/cm, and positive slopes (corresponding to potential phase rolling) were optimized between $\tan(0.04)$ and $\tan(0.25)$ cycles/cm. A field was determined as undergoing theta phase precession or rolling if a significant model was found within the negative or positive range of slopes, respectively ($p < 0.05$, permutation test). The number of phase precession/rolling cycles in every field was estimated by $a\Delta x$, where a is the precession/rolling slope, and Δx is the spatial distance between the first and last spike within the field.

A cycle randomization test was developed to assess the hypothesis of “within-cycle” phase rolling. For a tested place field, the phase and position of every spike within each theta cycle were randomized, yielding a set of surrogate phase-position pairs. For every spike, the surrogate pair was generated by randomly drawing a new time point within the cycle from a uniform distribution. The spike was assigned a new phase and position, corresponding to the phase and position values that actually occurred at that time point (Fig. 3B, gray lines). Thus, cycle randomization preserved the phase-position relations within every cycle. The randomization was conducted for every spike independently 1000 times. For each of the 1000 surrogate datasets, the fit of the phase-position pairs to the original circular-linear model was computed, generating a null distribution. The probability to obtain the original or higher fit under the null

hypothesis was estimated empirically from the null distribution. If the probability was lower than the α level, the within-cycle (null) hypothesis was rejected, and phase rolling was classified as “between-cycle.” As an independent check, the intra-cycle spike phase randomization test was applied to estimate theta phase precession. Of all CA1 PYR place fields, 772/1564 (49%) exhibited between-cycle phase precession, a fraction not consistently different from all fields with precession, 799/1564 (51%, $p = 0.58$, G test).

Statistical analyses

In all statistical tests used in this study, a significance threshold of $\alpha = 0.05$ was used. All descriptive statistics (n , median, IQR) can be found in Results and figure legends. To estimate whether a given fraction was smaller or larger than expected by chance, an exact binomial test was used. Differences between the proportions of observations of two categorical variables were tested with a likelihood ratio (G) test of independence. Differences between two group medians were tested with Mann–Whitney U test. Differences between medians of three groups were tested with Kruskal–Wallis test. Uniformity of the distribution of circular parameters was tested with Rayleigh’s likelihood-ratio test. Differences between the circular medians of two groups were tested with Wheeler’s nonparametric two-sample test. Rank (Spearman’s) and partial rank correlation coefficients were tested using permutation tests. In cases of multiple comparisons, Bonferroni’s correction was employed.

Table 2. Phase precession and rolling occurrence in every experimental animal

Category	Cell type	mC41	mA234	mP23	mDS1	mDS2	Sum
Active units	PYR	557	446	81	54	790	1928
	INT	212	135	26	13	155	541
Units with fields	PYR	320 (57%)	191 (43%)	32 (40%)	14 (26%)	462 (58%)	1019 (53%)
	INT	71 (33%)	56 (42%)	13 (50%)	3 (23%)	64 (41%)	207 (38%)
Fields	PYR	485	309	53	23	694	1564
	INT	80	70	19	3	89	261
Fields with phase precession	PYR	252 (52%)	171 (55%)	28 (53%)	12 (52%)	336 (48%)	799 (51%)
	INT	9 (11%)	2 (2.8%)	2 (10%)	0	3 (3.4%)	16 (6.1%)
Fields with between-cycle precession	PYR	241 (50%)	169 (55%)	26 (49%)	12 (52%)	324 (47%)	772 (49%)
	INT	8 (10%)	1 (1.4%)	2 (10%)	0	3 (3.4%)	14 (5%)
Fields with phase rolling	PYR	128 (26%)	106 (34%)	19 (35%)	10 (43%)	277 (40%)	540 (34%)
	INT	20 (25%)	18 (26%)	10 (53%)	1 (33%)	31 (35%)	80 (31%)
Fields with between-cycle phase rolling	PYR	60 (12%)	40 (13%)	7 (13%)	4 (17%)	129 (19%)	240 (15%)
	INT	7 (8.7%)	8 (11%)	0	0	10 (11%)	25 (9.6%)

Table 3. Number of PYR place fields co-exhibiting phase rolling and precession or phase rolling and lock

	Rolling	No rolling
Phase rolling vs phase precession (n.s.)		
Precession	278	521
No precession	262	503
Phase rolling vs phase lock***		
Phase lock	436	879
No phase lock	104	145

There is no consistent association between phase rolling and precession (n.s.: $p = 0.82$, G test). There is an association between phase rolling and phase lock (***) $p < 0.001$, G test).

Results

CA1 hippocampal cells undergo theta phase rolling

To quantify the relations between spike timing and the phase of the ongoing theta oscillations, we performed high-density extracellular recordings as five mice ran back and forth on a 150-cm-long linear track. Overall, the mice ran 167 [131.5 200.24] trials per session (median [IQR] of 97 sessions; Fig. 1A). We recorded a total of 6570 well-isolated units from hippocampal region CA1 of the animals. Of these, 5661 were putative pyramidal cells (PYR) and 909 were interneurons (INT; Table 1). Here, we focus on 1928/5661 (34%) PYRs and 541/909 (60%) INTs which were active on the linear track and exhibited stable spatial firing rate patterns across trials, henceforth referred to as “active units.” Most active units exhibited increased firing rates in a specific region of the track (Fig. 1B). The peak on-track firing rate was 8.3 [3.94 16.06] spikes/s for PYR and 32 [7.13 53.26] spikes/s for INT ($p = 3.53 \times 10^{-211}$, Mann–Whitney U test). Previous work showed that INT change their firing rate according to position, exhibiting “on” and “off” regions on the track (Maurer et al., 2006; Ego-Stengel and Wilson, 2007; Wilent and Nitz, 2007; Hangya et al., 2010). We therefore identified “place fields” in both PYR and INT as regions spanning 15–100 cm in which firing rate increased compared with the on-track spontaneous firing rate ($p < 0.05$, Bonferroni-corrected Poisson test). Place fields were identified in 1019/1928 (53%) of the active PYR and in 207/541 of the active INT (38%; Fig. 1C), yielding a total of 1564 PYR and 261 INT fields. The fraction of units with one or more fields was larger in PYR than in INT ($p = 0.00029$, G test of independence). Considering all active units, PYR had 0.69 ± 0.017 place fields per unit, while INT had 0.48 ± 0.029 place fields per unit (mean \pm SEM; $p = 3.57 \times 10^{-10}$, U test; Fig. 1Da). Place fields spanned 42 [28 58] cm in PYR, and were smaller in INT, spanning 30 [20 40] cm ($p = 1.2 \times 10^{-19}$, U test; Fig. 1Db). The in-field firing rate gain was higher among PYR (5.7 [1.8 21])

than among INT (1.3 [1.1 1.6]; $p = 4.5 \times 10^{-56}$, U test). Within place fields, PYR tended to fire slightly after the theta trough (mean \pm SD: $1.26\pi \pm 1.93\pi$ rad; $p = 1.9 \times 10^{-17}$, Rayleigh test), while INT tended to fire earlier ($p = 2.22 \times 10^{-16}$, Wheeler’s test), slightly before the theta trough ($0.85\pi \pm 1.36\pi$ rad; $p = 6.1 \times 10^{-19}$, Rayleigh test; Fig. 1E). To conclude, in mouse CA1, spatial regions with increased firing rates (“place fields”) were observed in both PYR and INT. However, PYR place fields were larger and exhibited higher in-field firing rate gain.

Many place fields exhibit theta phase precession (O’Keefe and Recce, 1993; Skaggs et al., 1996; Harvey et al., 2009), in which spikes occur earlier in consecutive theta cycles as the animal advances within the place field (Fig. 2A). To quantify precession, we fitted a circular-linear model to the instantaneous theta phase of each spike and the spatial position of the animal at spike time (Schmidt et al., 2009; Kempter et al., 2012). For every place field (1564 PYR and 261 INT fields), the slope a of a circular-linear model was varied systematically and the resultant length (R) of the residuals was calculated (Fig. 2D). The slope of the model was determined by optimizing the fit to the data. Of the PYR with place fields, 799/1564 (51%) fields exhibited theta phase precession ($p < 0.05$, permutation test), a fraction higher than expected by chance ($p < 1.11 \times 10^{-16}$, exact binomial test). In contrast, only 16/261 (6%) of the INT fields exhibited precession, a fraction not higher than expected by chance ($p = 0.24$, binomial test) and smaller than among PYR ($p < 2.93 \times 10^{-10}$, G test; Fig. 2E). Thus, theta phase precession was observed in about half of the PYR place fields but not in INT. These observations expand previous work (Maurer et al., 2006; Ego-Stengel and Wilson, 2007), showing that INT undergo precession specifically in regions corresponding to place fields of upstream PYR.

In addition to phase precession, we found that many fields exhibited a positive slope of phase changes: spikes occurred at a later theta phase on one cycle, compared with the previous cycle (Fig. 2B,C). Thus, spike phase shifted forward as the animal traversed the place field. We term this phenomenon, which is opposite in direction to theta phase precession, theta “phase rolling.” To quantify theta phase rolling, we employed the same circular-linear model fitting procedure used for quantifying phase precession, extending the range of allowed slopes to positive values (Fig. 2D). Studying these plots, three categories of slopes could be observed: (1) negative slopes, corresponding to phase precession; (2) horizontal (zero) slopes, corresponding to locking of spikes to a specific theta phase; and (3) positive slopes, corresponding to phase rolling. Some fields exhibited several fit peaks, implying the co-occurrence of spike phase lock, precession and

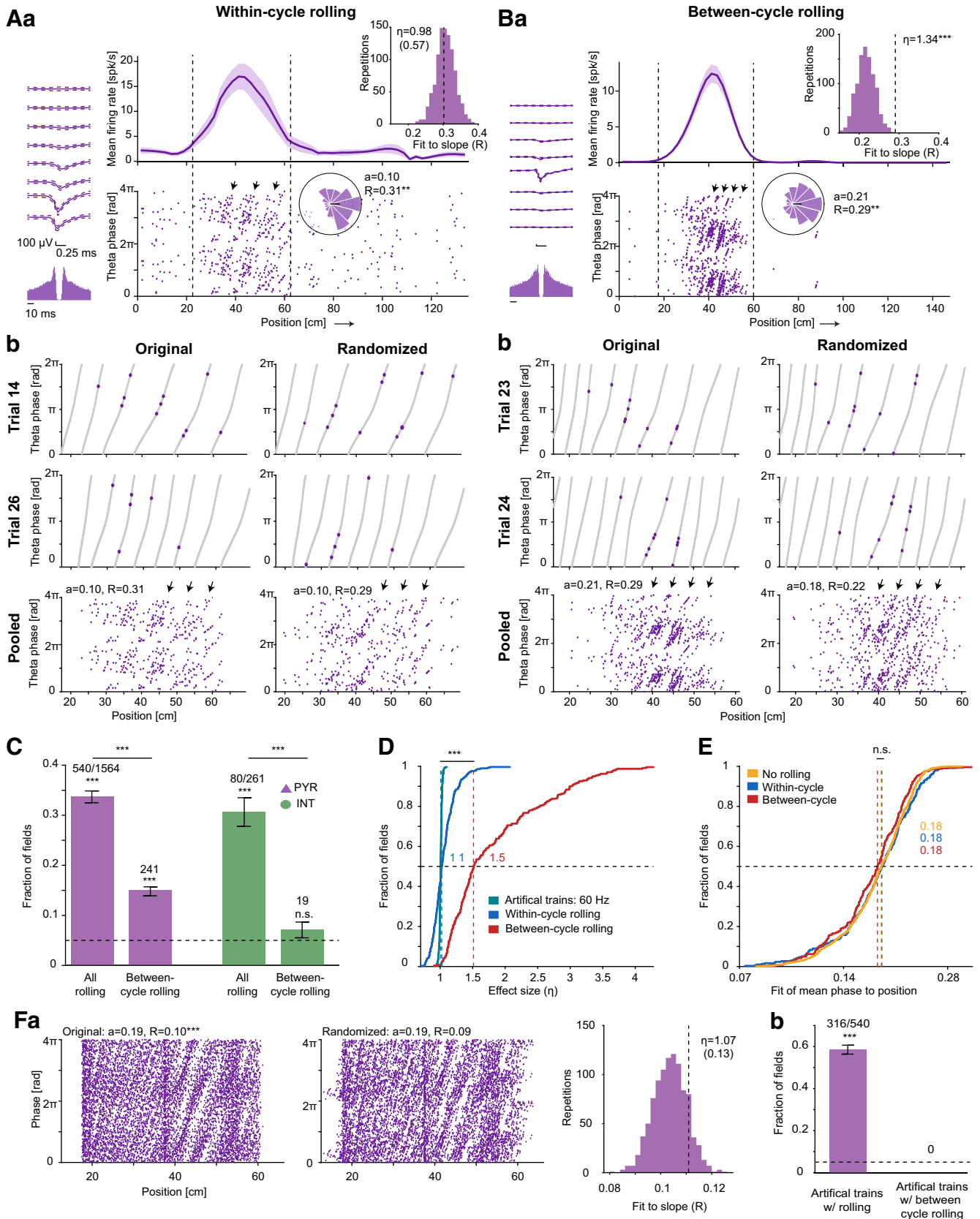


Figure 3. Phase rolling occurs within and between theta cycles. **A**, A PYR exhibiting within-cycle phase rolling (recorded during 26 same-direction trials). **a**, All conventions are the same as in Figure 2B. Top inset, To detect fields undergoing “between-cycle” phase rolling, the phase and position of every spike were randomized within each theta cycle (see panel **Ab**, right vs left columns). The fit of the original and randomized spikes to a rolling model was then calculated. The fits of the randomized spikes reflect the null, “within-cycle” distribution. In this example, the fit of the original spikes to the rolling model (vertical dashed line) is not higher than expected under the null hypothesis ($p = 0.56$, randomization test). Therefore, phase rolling is classified as within-cycle. **b**, Demonstration of one repetition of the phase-randomization test. Diagonal gray lines represent the continuous theta phase: spikes are randomized only along these lines.

rolling. To examine rolling even in fields with strong phase lock or precession, we performed the circular-linear model fitting procedure for positive slopes separately. Theta phase rolling occurred in 540/1564 (35%) of the PYR fields and in 80/261 (31%) of the INT fields ($p < 0.05$, permutation test; Fig. 2E). Both fractions were above expected by chance ($p < 1.11 \times 10^{-16}$, binomial test). Over the five mice tested, phase rolling prevalence was limited to the 26–43% range in PYR fields and to the 25–53% range in INT fields (Table 2). Unlike precession, the prevalence of phase rolling did not differ consistently between PYR and INT fields ($p = 0.38$, G test). Some fields co-exhibited phase lock, precession and rolling (Table 3). The occurrence of phase rolling and precession was not consistently associated ($p = 0.82$, G test). However, the occurrence of rolling was associated with the occurrence of phase lock ($p = 0.0097$, G test). In sum, theta phase rolling is a newly described phenomenon observed in about a third of the place fields in CA1.

Phase rolling occurs within and between theta cycles

The phenomenon of theta phase rolling may be of two types. First, in a cell with inter-spike intervals shorter than the theta cycle duration, consecutive spikes that occur during the same theta cycle will always occur at larger theta phases. This results in trivial theta phase rolling. Furthermore, if theta phase is locked to a specific position across multiple trials (Agarwal et al., 2014), phase rolling will appear whenever spikes are pooled over trials, even if every cycle includes only one spike. Together, we term such phase rolling as occurring “within-cycle.” Second, phase rolling can also occur between theta cycles, if individual spikes (or spike bursts) in consecutive theta cycles occur at consecutively larger theta phases: in the same trial, or in different trials. We term this “between-cycle” phase rolling. Any observed phase rolling may originate from within-cycle rolling only, between-

cycle rolling only, or both. Since within-cycle phase rolling can arise trivially while between-cycle cannot, we aimed to focus on between-cycle phase rolling.

To determine whether place fields exhibit nontrivial, “between-cycle” rolling, we developed a cycle randomization test. In the test, the phase and position of every spike are randomly drawn from the phases and positions that actually occurred in the relevant theta cycle (Fig. 3A,B, gray lines), generating surrogate phase-position pairs. The fit of the surrogate pairs to the original circular-linear rolling model is then computed. Because of the randomization, within-cycle phase-position relations are preserved, whereas relations between spikes occurring at distinct theta cycles are disrupted. If the probability to obtain the fit of the original spikes is lower than expected under the “within-cycle” (null) hypothesis, phase rolling is classified as “between-cycle.” Of all CA1 place fields, 241/1564 (15%) of PYR fields and 19/261 (7%) of INT fields exhibited between-cycle phase rolling (Fig. 3C). In PYR, the fraction of between-cycle phase rolling was above expected by chance ($p < 1.11 \times 10^{-16}$, exact binomial test), but smaller than the fraction of all phase rolling fields ($p < 3.33 \times 10^{-16}$, G test). In INT, the fraction of between-cycle phase rolling was not above expected by chance ($p = 0.067$, binomial test). The effect size η of between-cycle rolling was estimated by the fit of each rolling field (R), divided by the median fit over all cycle randomizations. η of PYR fields undergoing between-cycle rolling (1.5 [1.2 2]) was larger than that of within-cycle rolling fields (1 [0.94 1.1]; $p = 1.4 \times 10^{-63}$, Bonferroni-corrected Kruskal–Wallis test; Fig. 3D). To conclude, rolling in INT occurs exclusively within cycles. In contrast, in over a third of the phase rolling PYR fields, theta phase rolling occurs between cycles.

Two independent tests were used to determine whether fields identified by cycle randomization undergo “trivial” rolling. First, we estimated the lock of instantaneous phase to position across trials of each field. If rolling occurs mainly within-cycles, fields undergoing rolling would be expected to exhibit stronger lock to position. However, the mean fit of instantaneous lock to position did not differ consistently between rolling and nonrolling fields (nonrolling fields median [IQR]: 0.18 [0.15 0.21]; within-cycle rolling fields: 0.18 [0.15 0.21]; between-cycle rolling fields: 0.18 [0.15 0.2]; $p = 0.07$, Kruskal–Wallis test; Fig. 3E). Second, to assess whether phase-position relations suffice to generate rolling, we constructed artificial spike trains that fire at fixed intervals of 60 Hz, interposed on phase and position data of every real rolling field (Fig. 3F). We then conducted the circular-linear analysis and cycle randomization test, exactly as for the real spike trains. Phase rolling was detected in 316/540 (59%) of the artificial trains, above expected by chance ($p < 1.11 \times 10^{-16}$, binomial test). However, none of the artificial trains exhibited between-cycle rolling (Fig. 3Fb). Furthermore, effect sizes in fields undergoing between-cycle rolling (1.5 [1.3 2.2]) were larger than in fields with 60-Hz artificial spike trains (1 [1 1], $p = 5 \times 10^{-84}$, Bonferroni-corrected Kruskal–Wallis test; Fig. 3D). Thus, phase lock to position does not predict between-cycle rolling, and high firing rate alone does not generate between-cycle rolling.

An obvious limitation of the cycle randomization test is disruption of the ISI structure of spikes within individual theta cycles. To evaluate the prevalence of between-cycle rolling in a manner that maximally conserves the ISI structure, we applied a pattern jitter test to all spikes in every place field (Harrison and Geman, 2009). Spikes with ISI ≤ 10 ms were grouped together, and the groups were jittered within a window of up to 126 ms, representing the mean duration of a single theta cycle (Fig. 4A).

Top and middle, Original spikes and corresponding phase-randomized spikes in two example trials. Bottom, Original (left) and phase-randomized (right) spikes, pooled across all trials. In this example, randomization does not disrupt phase rolling. **B**, A PYR exhibiting between-cycle phase rolling. All conventions are the same as in panel **A**. **a**, The unit was recorded during 46 same-direction trials. Top inset, The fit of the original spikes to the rolling model is higher than expected under the within-cycle hypothesis ($p < 0.001$). **b**, The original spikes (left column) exhibit a higher fit than the phase-randomized spikes (right column). **C**, CA1 cells exhibit both within-cycle and between-cycle phase rolling. “All rolling”: fields with phase rolling ($p < 0.05$, permutation test). “Between-cycle rolling”: fields with phase rolling, for which the within-cycle hypothesis was rejected ($p < 0.05$, cycle randomization test). Horizontal dashed lines show chance level (0.05), and error bars show SEM. In PYR, the fraction of phase rolling fields is above chance for both conditions ($***p < 0.001$, binomial test). In INT, the fraction of rolling fields, but not the fraction of between-cycle rolling fields, is above expected by chance (n.s.: $p = 0.067$). The fraction of PYR with phase rolling is larger than the fraction of fields with between-cycle phase rolling ($***p < 0.001$, G test). **D**, The cycle-randomization effect size (η) is larger in fields undergoing between-cycle rolling than in fields undergoing within-cycle rolling, and η of artificial spike trains is smaller than that of between-cycle rolling fields ($***p < 0.001$, Bonferroni-corrected Kruskal–Wallis test). Vertical dashed lines show group medians, and horizontal dashed line indicates 50% of the fields. **E**, The mean fit of instantaneous phase to position does not differ consistently between rolling and nonrolling fields (n.s.: $p = 0.07$ Kruskal–Wallis test). Vertical dashed lines show group medians, and horizontal dashed line indicates 50% of the fields. **F**, Artificial spike trains that fire at fixed intervals of 60 Hz were interposed on rolling-fields phase and position data. **a**, Artificial spike trains interposed on an example place field (same as in panel **B**). The artificial train exhibited rolling ($p < 0.05$, permutation test), which was determined as within-cycle ($p > 0.05$, cycle randomization test). **b**, Artificial trains were interposed on data from all PYR fields undergoing phase rolling ($n = 540$). Many artificial fields exhibited phase rolling ($***p < 0.001$, binomial test). No artificial fields exhibited between-cycle rolling ($p > 0.05$, permutation test). Horizontal dashed line shows chance level (0.05); error bars, SEM.

Spike groups were then interval-jittered 1000 times to generate a null distribution, and the probability to obtain the original (or higher) fit under the null hypothesis was estimated empirically from the null distribution. If the probability was lower than the α level, the within-cycle (null) hypothesis was rejected, and phase rolling was classified as “between-cycle.” Out of 1564 PYR fields, 233 (15%) exhibited between-cycle phase rolling according to the pattern jitter method, a fraction higher than expected by chance ($p < 1.11 \times 10^{-16}$, exact binomial test). The fraction of fields exhibiting between-cycle rolling according to pattern jitter was not consistently different from that yielded by cycle randomization (241 fields, 15%; $p = 0.73$, G test; Fig. 4B). 191/233 (79%) fields exhibited between-cycle rolling according to pattern jitter and to cycle randomization (chance level, 2.3%; $p < 1.11 \times 10^{-16}$, exact binomial test). To test the sensitivity of the pattern jitter results, we repeated the analysis with three other ISI durations (6, 8, 12 ms) and two other windows (half-cycle: 63 ms; double cycle: 252 ms; Fig. 4C). In all cases, the fraction of fields exhibiting between-cycle rolling was above chance ($p < 1.11 \times 10^{-16}$, exact binomial test). Thus, an alternative randomization method which preserves the ISI structure yields similar results to the cycle randomization method.

Theta phase rolling is a rapid phase change

To characterize between-cycle theta phase rolling, we compared several properties of between-cycle phase rolling and phase precession (see example units in Figs. 2A, 5A, recorded simultaneously on the same shank). The fit of spikes to the circular-linear model was 0.24 [0.18 0.31] in PYR fields undergoing precession, compared with 0.14 [0.11 0.18] in PYR fields undergoing phase rolling ($p = 7.42 \times 10^{-51}$, U test; Fig. 5B). Compared with precession, between-cycle phase rolling exhibited a much faster slope with respect to spatial position (Fig. 5C). In PYR fields, phase rolling slope was 0.15 [0.068 0.19] cycles/cm, while precession slope size was 0.021 [0.015 0.03] cycles/cm ($p = 2.16 \times 10^{-112}$, U test). The variance of slope size was higher for phase-rolling fields than for fields exhibiting phase precession ($p = 0.002$, resampling test). Corresponding to the difference in slope size, spiking underwent multiple phase rolling cycles in every PYR place field (6.4 [2.7 11] cycles/field; Fig. 5D). The occurrence of multiple rolling cycles is in sharp contrast to precession, in which spikes underwent less than a single cycle of precession within every field (0.75 [0.57 1] cycles/field; $p = 3.86 \times 10^{-102}$, U test). Thus, compared with theta phase precession, between-cycle phase rolling is a faster phase change, spanning multiple cycles per field.

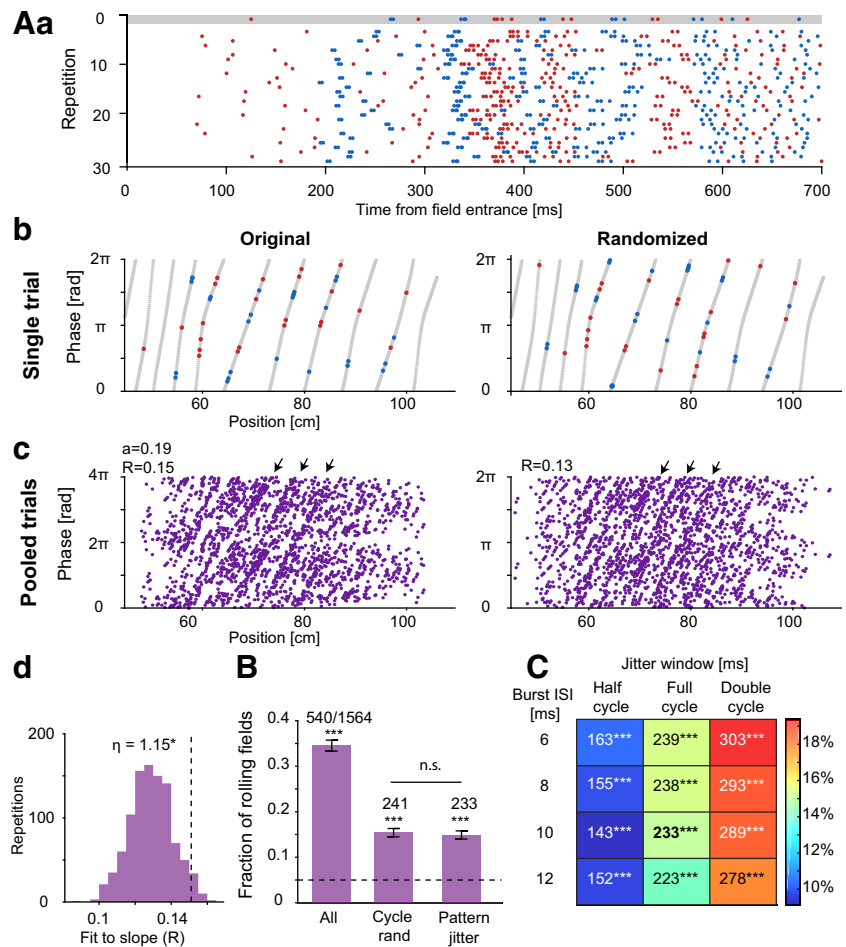


Figure 4. Pattern jitter preserves ISI structure and detects between-cycle rolling. **A**, Demonstration of the pattern jitter method for an example PYR (same unit as in Fig. 2B). **a**, Spike times in a single trial; every dot represents a spike. The original spike times are highlighted in gray. Jittered spike patterns are colored in red and blue, according to the ISI-based grouping. Each group is interval-jittered monolithically, under the constraint that the order of adjacent groups cannot be swapped. **b**, Spike phase as a function of position in the example trial (same as in **a**). Left, Original spikes (corresponding to the top row in **a**). Right, An example pattern jitter instantiation of the same trial. **c**, Spike phase as a function of position, pooled over all trials. Left, Original spikes. Right, Example repetition (same as in **b**). **d**, Distribution of rolling fit values (R) for pattern jittered spikes. Dashed line: rolling fit of original spikes. The fit of the original spikes to rolling model is higher than expected under the within-cycle hypothesis ($p < 0.05$). **B**, PYR fields exhibit between-cycle phase rolling according to the pattern jitter test. “All rolling”: fields with phase rolling ($p < 0.05$, permutation test). “Cycle rand”: fields with phase rolling, for which the within-cycle hypothesis was rejected based on the cycle randomization test ($p < 0.05$). “Pattern jitter”: fields with phase rolling, for which the within-cycle hypothesis was rejected based on the pattern jitter test ($p < 0.05$). Dashed line shows chance level (0.05). Error bars, SEM. The fraction of phase rolling fields is above chance in all three conditions (** $p < 0.001$, exact binomial test). **C**, Pattern jitter sensitivity analysis. Matrix shows the fraction of phase rolling fields following pattern jitter with various burst ISI lengths and jitter windows. Full cycle, 126 ms. Numbers denote the number of PYR fields undergoing between-cycle rolling following pattern jitter. Colors represent fractions out of all PYR fields ($n = 1564$). The fraction of phase rolling fields is above chance in all conditions (** $p < 0.001$, exact binomial test).

Rolling slope variance could originate from behavioral and anatomic differences within or between sessions. To examine whether precession and rolling slopes are stable over same-session trials, we divided the trials in every session into “early” and “late.” The precession slopes in the two halves of the session were correlated (747 fields, $cc: 0.48$, $p = 0.002$, permutation test), and did not differ consistently ($p = 0.79$, Wilcoxon’s paired signed-rank test; Fig. 5E). Similarly, rolling slopes were correlated between the two halves (241 fields, $cc: 0.3$, $p = 0.002$), and did not differ consistently ($p = 0.22$). To examine possible anatomic sources of variability, we accumulated all possible pairs of between-cycle rolling fields (28 920 pairs) over all sessions. For every pair, we calculated the pairwise slope difference. Field pairs were split

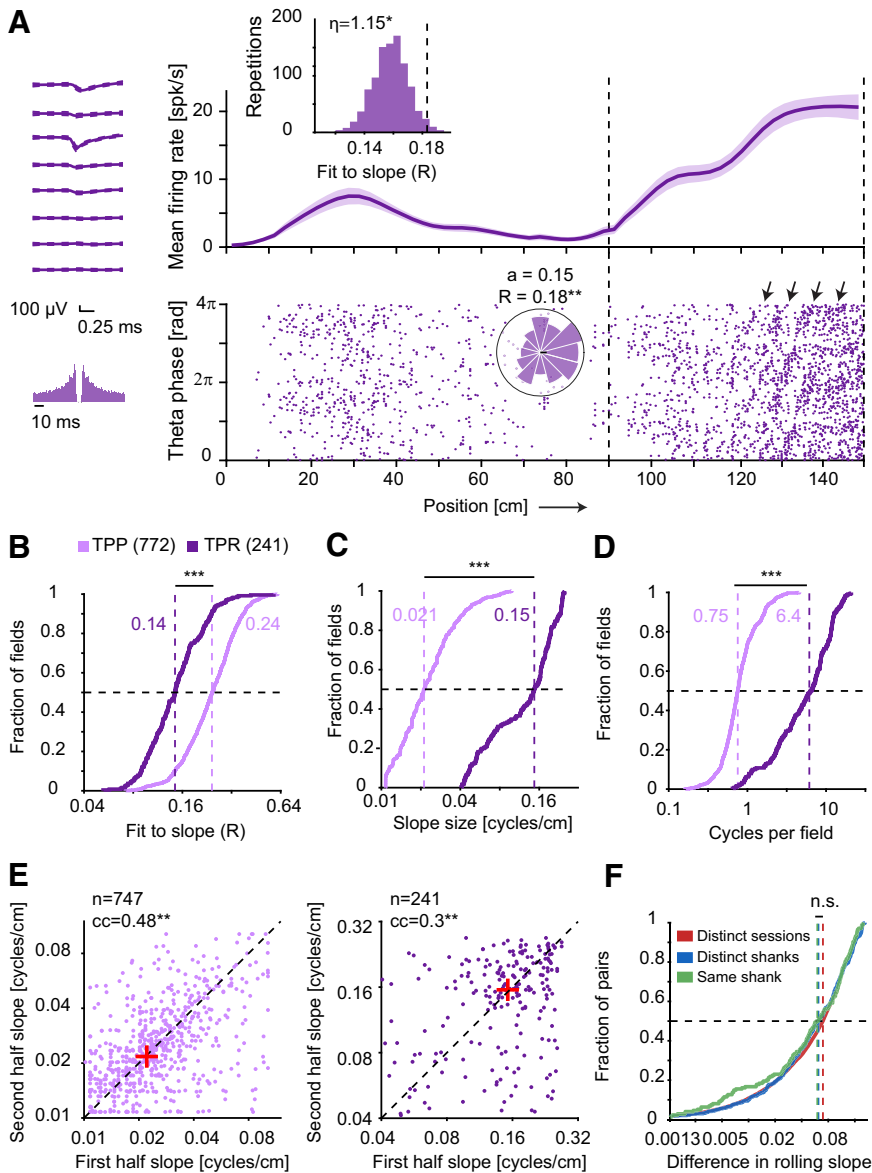


Figure 5. Theta phase rolling exhibits higher spatial fidelity than phase precession. **A**, An example PYR undergoing theta phase rolling, recorded simultaneously with the precessing PYR depicted in Figure 2B. All conventions are the same as in Figure 2B. **B**, The resultant length R is smaller for theta phase rolling than for phase precession ($***p < 0.001$, U test). Here and in panels **C**, **D**, cumulative distributions are shown only for fields with between-cycle phase changes (precession/rolling: $p < 0.05$, permutation test; between-cycles: $p < 0.05$, cycle randomization test). The number of fields in each group is indicated in parentheses. TPP, theta phase precession; TPR, theta phase rolling. Vertical dashed lines show group medians, and horizontal dashed lines indicate 50% of the fields. **C**, In PYR, theta phase rolling slope size is larger than phase precession slope size (absolute value: $***p < 0.001$, U test). **D**, Theta phase rolling exhibits more cycles per field than phase precession ($***p < 0.001$, U test). **E**, Precession (left) and rolling (right) slopes estimated based on trials in the first and second halves of the same session are correlated ($**p < 0.01$, permutation test) and not different from each other (rolling: $p = 0.22$, precession: $p = 0.79$, Wilcoxon's signed-rank test). The + sign shows the medians of both groups. The diagonal dashed line is the identity line. **F**, Pairs of phase rolling fields recorded during separate sessions, during the same session on distinct shanks, and on same shank do not exhibit disparate pairwise slope differences ($p = 0.49$, Kruskal–Wallis test).

into three mutually exclusive groups: (1) recorded during distinct sessions (28,313 pairs); (2) recorded during the same session but on distinct shanks (433 pairs); and (3) recorded during the same session and on the same shank (174 pairs). There was no disparity in the pairwise slope difference between the three groups (median [IQR] in different sessions: 0.07 [0.028 0.12]; different shanks: 0.062 [0.027 0.12]; same shank: 0.06 [0.025 0.11]; $p = 0.49$, Kruskal–Wallis test; Fig. 5F). To conclude, while rolling slope sizes are more variable than precession slope sizes, rolling slope appears to be

consistent between trials. Furthermore, locally co-recorded units do not appear to show particularly similar slopes.

Phase rolling occurs in larger place fields and is centered around a distinct firing phase

To understand what differentiates PYR fields that undergo between-cycle phase rolling from fields that do not, we first considered the possible contribution of microcircuits along the deep-superficial axis of CA1 (Mizuseki et al., 2011; Geiller et al., 2017; Sharif et al., 2021). Fields were grouped to bins of 5 μ m along the depth of the pyramidal layer, and the fraction of between-rolling fields out of all fields was calculated within each bin. The fraction of fields exhibiting between-cycle rolling was not consistently correlated with depth ($cc = -0.1$, $p = 0.43$, permutation test). Furthermore, there was no consistent correlation between rolling slope size and depth ($cc: 0.086$, $p = 0.3$, permutation test). Thus, phase rolling prevalence and slope do not vary consistently along the deep-superficial axis of CA1.

Next, we assessed the correlation between a host of cellular-network features and the occurrence of phase rolling. A total of 21 features were considered: behavioral, in-field LFP, spiking, network, on-track spiking, in-field spiking, and in-field spike-LFP features (Table 4; Fig. 6A). A multiple regression analysis of these features explained part of the variance associated with the occurrence of between-cycle phase rolling ($R^2 = 0.14$, $p = 0.00067$, permutation test). Next, for each feature, the rank cc and the partial cc (pcc) were computed and Bonferroni corrected for multiple comparisons. Five features were consistently correlated with the occurrence of between-cycle phase rolling. First, on-track firing rates were not consistently correlated with phase rolling occurrence ($cc: 0.042 \pm 0.0024$, $p = 0.096$), but did exhibit consistent partial correlation with rolling occurrence (pcc: 0.095 ± 0.0024 , $p = 0.00067$). Second, phase rolling occurrence was correlated with the fit of spikes to the rolling slope (pcc: 0.31 ± 0.002 , $p = 0.00067$, permutation test). The fit of spikes to the rolling slope

was higher in fields with between-cycle phase rolling, 0.14 [0.11 0.18] compared with 0.12 [0.089 0.16] in other fields ($p = 8.71 \times 10^{-11}$, U test; Fig. 6B). This observation is consistent with a monotonous relation between phase rolling fit and the probability of rolling detection. Third, phase rolling occurrence was negatively correlated with spike phase lock fit (pcc: -0.1 ± 0.0026 , $p = 0.00067$). The fit (R) of spikes to a fixed theta phase was 0.11 [0.073 0.15] in fields with phase rolling and 0.13 [0.083 0.2] in

Table 4. Theta phase rolling occurrence is correlated with in-field spike-LFP features and with field size

Feature	Feature	cc ± SEM	cc <i>p</i> -value	pcc ± SEM	pcc <i>p</i> -value
Behavioral features	Number of trials	−0.036 ± 0.0023	0.17	0.044 ± 0.0022	0.1
	In-field speed (cm/s)	−0.018 ± 0.0022	0.47	−0.032 ± 0.0022	0.2
	In-field speed SD (cm/s)	−0.0083 ± 0.0025	0.75	0.037 ± 0.0028	0.13
In-field LFP features	Phase-position lock (R)	−0.057 ± 0.0027	0.026	−0.0065 ± 0.0025	0.79
	SD of phase-position lock	0.066 ± 0.0026	0.011	0.0041 ± 0.0025	0.87
Spiking features	Spike width (ms)	0.017 ± 0.0027	0.5	−0.012 ± 0.0028	0.61
	Burst index	0.05 ± 0.0026	0.054	0.021 ± 0.0027	0.42
	Ripple firing rate gain	−0.039 ± 0.0028	0.1	−0.045 ± 0.0026	0.079
	Non-theta immobility firing rate (spk/s)	0.032 ± 0.0027	0.2	−0.026 ± 0.0028	0.31
Network features	Postsynaptic units	0.096 ± 0.0025	0.0013	0.021 ± 0.0022	0.41
	Presynaptic INT	0.036 ± 0.0026	0.15	0.011 ± 0.0026	0.69
On track spiking features	Firing rate (spk/s)	0.042 ± 0.0024	0.096	0.095 ± 0.0024	0.00067
	Spatial information (bits/s)	0.037 ± 0.0025	0.15	0.05 ± 0.0029	0.042
In-field spiking features	Field firing rate gain	−0.016 ± 0.0029	0.55	0.0067 ± 0.0028	0.79
	Field size (cm)	0.1 ± 0.0024	0.00067	0.18 ± 0.0024	0.00067
In-field spike-LFP features	Spikes per theta cycle	0.068 ± 0.0022	0.008	0.057 ± 0.0027	0.033
	Spike lock to theta phase (R)	−0.12 ± 0.0024	0.00067	−0.1 ± 0.0026	0.00067
	Sine of preferred phase	−0.04 ± 0.0027	0.1	−0.087 ± 0.0028	0.00067
	Cosine of preferred phase	0.062 ± 0.0025	0.011	0.027 ± 0.0028	0.27
	Rolling fit (R)	0.16 ± 0.0023	0.00067	0.31 ± 0.002	0.00067
	Rolling slope (cycles/cm)	0.039 ± 0.0024	0.13	0.022 ± 0.0023	0.39

Correlation of between-cycle phase rolling occurrence with field features. cc, rank correlation coefficient; pcc, partial cc. Together, the 21 features considered explain 14% of the variance among fields with and without between-cycle phase rolling ($R^2 = 0.14$; $p = 0.00067$, permutation test). *P*-values for cc and pcc are uncorrected; features that exhibit significant correlation after Bonferroni correction for multiple comparisons (i.e., *p*-value smaller than 0.05/21) are marked in bold.

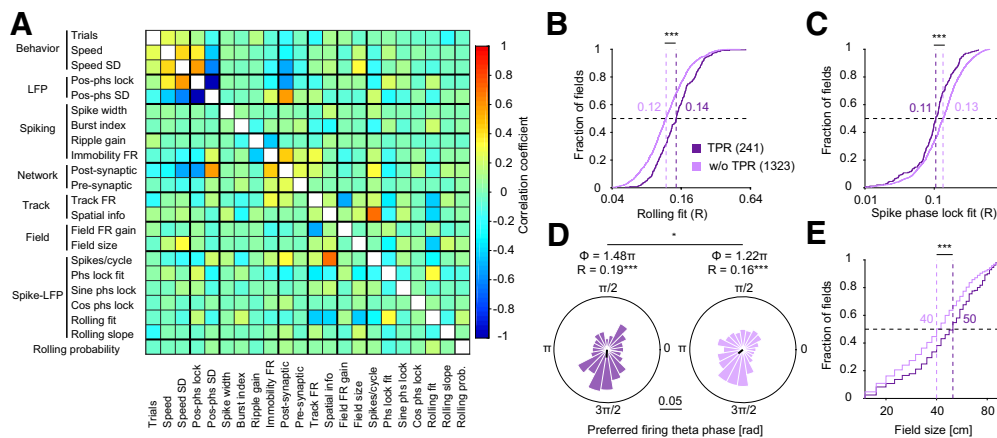


Figure 6. Theta phase rolling occurrence is correlated with field size. **A**, Matrix of pair-wise rank correlation coefficients between all 21 features tested for association with between-cycle phase rolling occurrence. The full name of every feature and details of correlation with phase rolling occurrence are detailed in Table 4. **B**, The fit of spikes to theta phase rolling slope is larger in fields with between-cycle phase rolling ($***p < 0.001$, *U* test). Here and in panels **C**, **E**, vertical dashed lines show group medians; the median of each group is indicated. **C**, The spike phase lock fit is smaller in fields with between-cycle phase rolling ($***p < 0.001$, *U* test). **D**, Preferred firing theta phase does not distribute uniformly in fields with and without between-cycle phase rolling ($*p < 0.05$, $***p < 0.001$, Rayleigh test). The preferred firing theta phase is different among fields with and without between-cycle rolling ($***p < 0.001$, Wheeler test). All conventions are the same as Figure 1E. **E**, Fields exhibiting between-cycle rolling are larger ($***p < 0.001$, *U* test).

fields without phase rolling ($p = 8.49 \times 10^{-7}$; Fig. 6C). Indeed, if spike theta phase shifts within the field, the fit to a horizontal line (phase lock) decreases. Fourth, phase rolling occurrence was associated with distinct preferred firing phases (sine of preferred phase: $pcc: -0.087 \pm 0.0028$, $p = 0.00067$). Specifically, fields with between-cycle phase rolling preferred firing at the middle of the rising theta cycle (mean ± SD: $1.48\pi \pm 1.83\pi$ rad, $R = 0.19$, $p = 0.00019$, Rayleigh test), while nonrolling fields exhibited locking to an earlier phase ($1.22\pi \pm 1.91\pi$ rad, $R = 0.16$, $p = 1.5 \times 10^{-15}$), slightly after the theta trough ($p = 0.01$, Wheeler test; Fig. 6D). Finally, phase rolling occurrence was correlated with place field size (pcc: 0.099 ± 0.0024 , $p = 0.00067$). Fields with phase rolling were 50 [34–62] cm, larger than fields without rolling (40 [28–58] cm; $p = 3.34 \times 10^{-5}$, *U* test; Fig. 6E). This suggests a relation between phase rolling and the way cells encode spatial position.

Discussion

We found that putative pyramidal cells (PYR) and interneurons (INT) in mouse hippocampal region CA1 exhibit a previously undescribed type of phase changes with respect to space, theta phase rolling. In phase rolling, spike phase shifts forward between theta cycles as a function of space: as the animal traverses the place field, spikes on distinct theta cycles occur at gradually later phases. Theta phase rolling is a fast phase change that tends to occur in larger fields.

Within-cycle versus between-cycle phase rolling

Theta phase rolling may appear because of the advancement of spikes with relation to theta phase either within or between cycles (Fig. 3). Within-cycle theta phase rolling can arise trivially, directly from the definition of phase, either if multiple spikes

occur within a given theta cycle, or if theta phase itself is similar at a given position across multiple trials (Agarwal et al., 2014). In addition to within-cycle rolling, phase rolling may occur between spikes in distinct theta cycles, i.e., at distinct spatial positions. To determine whether place fields undergo between-cycle rolling, a cycle randomization test was developed, which identified fields in which rolling could not be explained by the within-cycle hypothesis. The results of the cycle-randomization test were corroborated by a pattern-jitter test, and by analyzing artificial spike trains. Using both cycle randomization and pattern jitter, we found that a total of 15% of the PYR fields exhibited between-cycle rolling. However, this may be considered a lower bound on the prevalence of phase rolling, since other fields may have exhibited both types of rolling.

Possible functions of between-cycle phase rolling

Our results uncover a newly described phase change in which spikes shift to later theta phases as the animal moves forward in space. Previous studies have shown that a positive phase shift can follow the negative slope of phase precession in the second part of the place field (Yamaguchi et al., 2002; Wang et al., 2020). A positive phase shift was also described in other reports (Ego-Stengel and Wilson, 2007; Monaco et al., 2019). However, in the previous studies, positive phase changes exhibited slope sizes similar to those reported for precession. In contrast, the between-cycle phase rolling reported here is prevalent among PYRs (Fig. 3C) and, compared with phase precession, exhibits higher fidelity with respect to spatial position (Fig. 5).

Akin to place cell firing rates and to precession, theta phase rolling may contain information about the position of the animal. The instantaneous firing rate of a place cell indicates whether the animal is within the place field, and to some extent, where the animal is within the field (O'Keefe and Dostrovsky, 1971; Wilson and McNaughton, 1993; Brown et al., 1998; Moser et al., 2008). However, for single-peaked place fields, the instantaneous firing rate can only indicate that the animal is in one of two ranges. In place cells undergoing precession, the theta phase of spikes also contains information about position (O'Keefe and Recce, 1993; Skaggs et al., 1996), such that spike theta phase can indicate that the animal is within a single spatial range. The combination of theta phase with firing rate increases information about position (Jensen and Lisman, 2000; Reifenshtein et al., 2012). Analogous to precession, phase rolling is a position dependent signal. Thus, we hypothesize that rolling by itself may reduce uncertainty about animal position. Distinctly from precession, a given phase rolling phase corresponds to multiple possible regions in space. Restricting the potential position of the animal to several short ranges may aid in estimating the position of the animal.

Following the observation of between-cycle phase rolling, we asked whether and what is unique in fields undergoing phase rolling. Phase rolling occurrence was found to be correlated with field size (Table 4; Fig. 6). Previous work showed that place fields are smaller and precession is more informative in cue-poor environments (Sharif et al., 2021). The association between larger field size and phase rolling may suggest that precession and rolling are distinct phase changes, exhibited in different environments. In small and/or cue-rich environments, place fields are smaller, and spike theta phase accurately encodes position. However, in larger and/or cue-poor environments, which typically exhibit larger place fields, rolling might increase spatial

information by effectively partitioning the field into smaller subregions.

While the current study showed that phase rolling is correlated with animal position, we did not demonstrate that phase rolling contains spatial information or plays a causal role in spatial navigation. In future work, a functional role for rolling may be supported by a decoding analysis of animal position based on the instantaneous phase of phase-rolling fields, as has been previously done for precession (Jensen and Lisman, 2000). The functional role of rolling may be directly tested by manipulating spontaneous phase changes, or by inducing artificial phase changes and quantifying the influence on spatial behavior.

References

- Adrian ED, Zotterman Y (1926) The impulses produced by sensory nerve endings. *J Physiol* 61:465–483.
- Agarwal G, Stevenson IH, Berényi A, Mizuseki K, Buzsáki G, Sommer FT (2014) Spatially distributed local fields in the hippocampus encode rat position. *Science* 344:626–630.
- Azarfar A, Calcini N, Huang C, Zeldenrust F, Celikel T (2018) Neural coding: a single neuron's perspective. *Neurosci Biobehav Rev* 94:238–247.
- Barlow HB (1972) Single units and sensation: a neuron doctrine for perceptual psychology? *Perception* 1:371–394.
- Belluscio MA, Mizuseki K, Schmidt R, Kempter R, Buzsáki G (2012) Cross-frequency phase-phase coupling between θ and γ oscillations in the hippocampus. *J Neurosci* 32:423–435.
- Bialek W, Rieke F, de Ruyter van Steveninck RR, Warland D (1991) Reading a neural code. *Science* 252:1854–1857.
- Brown EN, Frank LM, Tang D, Quirk MC, Wilson MA (1998) A statistical paradigm for neural spike train decoding applied to position prediction from ensemble firing patterns of rat hippocampal place cells. *J Neurosci* 18:7411–7425.
- Buzsáki G, Draguhn A (2004) Neuronal oscillations in cortical networks. *Science* 304:1926–1929.
- Buzsáki G, Anastassiou CA, Koch C (2012) The origin of extracellular fields and currents — EEG, ECoG, LFP and spikes. *Nat Rev Neurosci* 13:407–420.
- Cei A, Girardeau G, Drieu C, Kanbi KE, Zugaro M (2014) Reversed theta sequences of hippocampal cell assemblies during backward travel. *Nat Neurosci* 17:719–724.
- Chase SM, Young ED (2007) First-spike latency information in single neurons increases when referenced to population onset. *Proc Natl Acad Sci U S A* 104:5175–5180.
- Csicsvari J, Hirase H, Czurkó A, Mamiya A, Buzsáki G (1999) Oscillatory coupling of hippocampal pyramidal cells and interneurons in the behaving rat. *J Neurosci* 19:274–287.
- deCharms RC, Zador A (2000) Neural representation and the cortical code. *Annu Rev Neurosci* 23:613–647.
- Diamantaki M, Coletta S, Nasr K, Zeraati R, Laturus S, Berens P, Preston-Ferrer P, Burgalossi A (2018) Manipulating hippocampal place cell activity by single-cell stimulation in freely moving mice. *Cell Rep* 23:32–38.
- Ego-Stengel V, Wilson MA (2007) Spatial selectivity and theta phase precession in CA1 interneurons. *Hippocampus* 17:161–174.
- Fee MS, Mitra PP, Kleinfeld D (1996) Automatic sorting of multiple unit neuronal signals in the presence of anisotropic and non-Gaussian variability. *J Neurosci Methods* 69:175–188.
- Frank LM, Brown EN, Wilson MA (2001) A comparison of the firing properties of putative excitatory and inhibitory neurons from CA1 and the entorhinal cortex. *J Neurophysiol* 86:2029–2040.
- Gaspar N, Eichler R, Stark E (2019) A novel low-noise movement tracking system with real-time analog output for closed-loop experiments. *J Neurosci Methods* 318:69–77.
- Geiller T, Fattahi M, Choi J-S, Royer S (2017) Place cells are more strongly tied to landmarks in deep than in superficial CA1. *Nat Commun* 8:14531.
- Graf ABA, Kohn A, Jazayeri M, Movshon JA (2011) Decoding the activity of neuronal populations in macaque primary visual cortex. *Nat Neurosci* 14:239–245.
- Gray CM, König P, Engel AK, Singer W (1989) Oscillatory responses in cat visual cortex exhibit inter-columnar synchronization which reflects global stimulus properties. *Nature* 338:334–337.

- Hafting T, Fyhn M, Bonnevie T, Moser MB, Moser EI (2008) Hippocampus-independent phase precession in entorhinal grid cells. *Nature* 453:1248–1252.
- Hangya B, Li Y, Muller RU, Czurkó A (2010) Complementary spatial firing in place cell-interneuron pairs. *J Physiol* 588:4165–4175.
- Harrison MT, Geman S (2009) A rate and history-preserving resampling algorithm for neural spike trains. *Neural Comput* 21:1244–1258.
- Hartley T, Lever C, Burgess N, O’Keefe J (2014) Space in the brain: how the hippocampal formation supports spatial cognition. *Philos Trans R Soc Lond B Biol Sci* 369:20120510.
- Harvey CD, Collman F, Dombeck DA, Tank DW (2009) Intracellular dynamics of hippocampal place cells during virtual navigation. *Nature* 461:941–946.
- Herreras O (2016) Local field potentials: myths and misunderstandings. *Front Neural Circuits* 10:101.
- Imaizumi K, Priebe NJ, Sharpee TO, Cheung SW, Schreiner CE (2010) Encoding of temporal information by Timing, rate, and place in cat auditory cortex. *PLoS One* 5:e11531–15.
- Jensen O, Lisman JE (2000) Position reconstruction from an ensemble of hippocampal place cells: contribution of theta phase coding. *J Neurophysiol* 83:2602–2609.
- Kadir SN, Goodman DFM, Harris KD (2014) High-dimensional cluster analysis with the masked EM algorithm. *Neural Comput* 26:2379–2394.
- Kempler R, Leibold C, Buzsáki G, Diba K, Schmidt R (2012) Quantifying circular-linear associations: hippocampal phase precession. *J Neurosci Methods* 207:113–124.
- Klausberger T, Magill PJ, Márton LF, Roberts JDB, Cobden PM, Buzsáki G, Somogyi P (2003) Brain-state- and cell-type-specific firing of hippocampal interneurons in vivo. *Nature* 421:844–848.
- Kohn A, Coen-Cagli R, Kanitscheider I, Pouget A (2016) Correlations and neuronal population information. *Annu Rev Neurosci* 39:237–256.
- Lever C, Kaplan R, Burgess N (2014) The function of oscillations in the hippocampal formation. In: *Space, time and memory in the hippocampal formation* (Derdikman D, Knierim JJ, eds), pp 303–350. Vienna: Springer.
- Maurer AP, Cowen SL, Burke SN, Barnes CA, McNaughton BL (2006) Phase precession in hippocampal interneurons showing strong functional coupling to individual pyramidal cells. *J Neurosci* 26:13485–13492.
- Maurer AP, Lester AW, Burke SN, Ferng JJ, Barnes CA (2014) Back to the future: preserved hippocampal network activity during reverse ambulation. *J Neurosci* 34:15022–15031.
- Mehta MR, Lee AK, Wilson MA (2002) Role of experience and oscillations in transforming a rate code into a temporal code. *Nature* 417:741–746.
- Mizuseki K, Diba K, Pastalkova E, Buzsáki G (2011) Hippocampal CA1 pyramidal cells form functionally distinct sublayers. *Nat Neurosci* 14:1174–1181.
- Monaco JD, De Guzman RM, Blair HT, Zhang K (2019) Spatial synchronization codes from coupled rate-phase neurons. *PLoS Comput Biol* 15:e1006741.
- Montemurro MA, Rasch MJ, Murayama Y, Logothetis NK, Panzeri S (2008) Phase-of-firing coding of natural visual stimuli in primary visual cortex. *Curr Biol* 18:375–380.
- Moser EI, Kropff E, Moser MB (2008) Place cells, grid cells, and the brain’s spatial representation system. *Annu Rev Neurosci* 31:69–89.
- Noked O, Levi A, Someck S, Amber-Vitos O, Stark E (2021) Bidirectional optogenetic control of inhibitory neurons in freely-moving mice. *IEEE Trans Biomed Eng* 68:416–427.
- O’Keefe J, Dostrovsky J (1971) The hippocampus as a spatial map. Preliminary evidence from unit activity in the freely-moving rat. *Brain Res* 34:171–175.
- O’Keefe J, Recce ML (1993) Phase relationship between hippocampal place units and the EEG theta rhythm. *Hippocampus* 3:317–330.
- Optican LM, Richmond BJ (1987) Temporal encoding of two-dimensional patterns by single units in primate inferior temporal cortex. III. Information theoretic analysis. *J Neurophysiol* 57:162–178.
- Pachitariu M, Steinmetz N, Kadir S, Carandini M, Kenneth DH (2016) Kilosort: realtime spike-sorting for extracellular electrophysiology with hundreds of channels. *bioRxiv*. doi: 10.1101/061481.
- Reich DS, Mechler F, Purpura KP, Victor JD (2000) Interspike intervals, receptive fields, and information encoding in primary visual cortex. *J Neurosci* 20:1964–1974.
- Reifenstein ET, Kempler R, Schreiber S, Stemmler MB, Herz AVM (2012) Grid cells in rat entorhinal cortex encode physical space with independent firing fields and phase precession at the single-trial level. *Proc Natl Acad Sci USA* 109:6301–6306.
- Rossant C, Kadir SN, Goodman DFM, Schulman J, Hunter MLD, Saleem AB, Grosmark A, Belluscio M, Denfield GH, Ecker AS, Tolias AS, Solomon S, Buzsáki G, Carandini M, Harris KD (2016) Spike sorting for large, dense electrode arrays. *Nat Neurosci* 19:634–641.
- Royer S, Zemelman BV, Losonczy A, Chance F, Magee JC, Buzsáki G (2012) Control of timing, rate and bursts of hippocampal place cells by dendritic and somatic inhibition. *Nat Neurosci* 15:769–775.
- Schmidt R, Diba K, Leibold C, Schmitz D, Buzsáki G, Kempler R (2009) Single-trial phase precession in the hippocampus. *J Neurosci* 29:13232–13241.
- Schmitzer-Torbert N, Jackson J, Henze D, Harris K, Redish AD (2005) Quantitative measures of cluster quality for use in extracellular recordings. *Neuroscience* 131:1–11.
- Sharif F, Tayebi B, Buzsáki G, Royer S, Fernandez-Ruiz A (2021) Subcircuits of deep and superficial CA1 place cells support efficient spatial coding across heterogeneous environments. *Neuron* 109:363–376.
- Siadatnejad S, Bale M, Petersen RS, Montemurro MA (2013) Phase-of-firing coding of dynamical whisker stimuli and the thalamocortical code in barrel cortex. *BMC Neurosci* 14:P279.
- Singer W (2018) Neuronal oscillations: unavoidable and useful? *Eur J Neurosci* 48:2389–2398.
- Skaggs WE, McNaughton BL, Wilson MA, Barnes CA (1996) Theta phase precession in hippocampal neuronal populations and the compression of temporal sequences. *Hippocampus* 6:149–172.
- Somogyi P, Klausberger T (2005) Defined types of cortical interneurone structure space and spike timing in the hippocampus. *J Physiol* 562:9–26.
- Souza BC, Tort ABL (2017) Asymmetry of the temporal code for space by hippocampal place cells. *Sci Rep* 7:8507.
- Stanley GB (2013) Reading and writing the neural code. *Nat Neurosci* 16:259–263.
- Stark E, Koos T, Buzsáki G (2012) Diode probes for spatiotemporal optical control of multiple neurons in freely moving animals. *J Neurophysiol* 108:349–363.
- Stark E, Eichler R, Roux L, Fujisawa S, Rotstein HG, Buzsáki G (2013) Inhibition-induced theta resonance in cortical circuits. *Neuron* 80:1263–1276.
- Tingley D, Alexander AS, Quinn LK, Chiba AA, Nitz D (2018) Multiplexed oscillations and phase rate coding in the basal forebrain. *Sci Adv* 4:eaar3230.
- Tsodyks MV, Skaggs WE, Sejnowski TJ, McNaughton BL (1996) Population dynamics and theta rhythm phase precession of hippocampal place cell firing: a spiking neuron model. *Hippocampus* 6:271–280.
- Turesson HK, Logothetis NK, Hoffman KL (2012) Category-selective phase coding in the superior temporal sulcus. *Proc Natl Acad Sci USA* 109:19438–19443.
- Van Der Meer MAA, Redish AD (2011) Theta phase precession in rat ventral striatum links place and reward information. *J Neurosci* 31:2843–2854.
- Vanderwolf CH (1969) Hippocampal electrical activity and voluntary movement in the rat. *Electroencephalogr Clin Neurophysiol* 26:407–418.
- Wang M, Foster DJ, Pfeiffer BE (2020) Alternating sequences of future and past behavior encoded within hippocampal theta oscillations. *Science* 370:247–250.
- Wilent WB, Nitz DA (2007) Discrete place fields of hippocampal formation interneurons. *J Neurophysiol* 97:4152–4161.
- Wilson MA, McNaughton BL (1993) Dynamics of the hippocampal ensemble code for space. *Science* 261:1055–1058.
- Yamaguchi Y, Aota Y, McNaughton BL, Lipa P (2002) Bimodality of theta phase precession in hippocampal place cells in freely running rats. *J Neurophysiol* 87:2629–2642.
- Ylinen A, Bragin A, Nádasdy Z, Jandó G, Szabó I, Sik A, Buzsáki G (1995) Sharp wave-associated high-frequency oscillation (200 Hz) in the intact hippocampus: network and intracellular mechanisms. *J Neurosci* 15:30–46.